Starch modified polyol-based hyperbranched polyurethane

Highlight

This chapter emphasizes the synthesis, characterization and property evaluation of tough, smart, biodegradable and biocompatible starch modified polyol based hyperbranched polyurethane (HPU) suitable for use in medical implant devices. The chapter depicts the synthesis of starch modified polyol, as a multifunctional moiety. This polyol is generated by hydrolysis of starch based epoxy resin. The polyol is subsequently used in synthesis of HPU, which is obtained via $A_x + B_y$ ($x, y \geq 2$) approach, without using any plasticizers or catalysts. The synthesized HPU is well characterized by various techniques. It exhibited combined attributes of remarkable mechanical properties and desired shape memory behavior at around body temperature. Moreover, cell proliferation and live/dead cell viability assays confirmed biocompatibility of the synthesized HPU. The chapter illustrates the overall results which indicated its potential as an advanced biomedical material.

Parts of this chapter are published in

[1] **Duarah, R.** and Karak, N. A starch based sustainable tough hyperbranched epoxy thermoset. *RSC Advances,* 5(79):64456-64465, 2015.

[2] **Duarah, R.**, Singh, Y. P., Mandal, B. B., and Karak, N. Sustainable starch modified polyol based tough, biocompatible, hyperbranched polyurethane with a shape memory attribute. *New Journal of Chemistry*, 40(6):5152-5163, 2016.

2.1. Introduction

Chapter 1 evidently stated that the development of tough, smart and biodegradable polyurethane(s) (PU) for diverse advanced applications is significant in today's material scenario [1]. The mere judicious alteration of the structures and compositions of the three reactants, *viz*., macroglycol, diisocyanate and chain extender presents scope to adjust the different chemical and physical attributes of PU [2, 3]. Thus, over the last two decades, the development of hyperbranched PU (HPU) with suitable composition and structure furnished with unique and functional attribute attracted substantial interest among researchers [4]. The globular, compact and non-entangled structure of such polymers with large number of active peripheral polar functional groups imparts them with exceptional attributes like low hydrodynamic diameter, high solubility, and low solution and melts viscosities [5, 6]. Such distinctive architectural structure of HPU leads to superior properties in comparison to its linear analog. However, despite such benefits, HPU still suffers from some demerits such as poor mechanical property etc. Such setbacks are dealt by integration of a long chain consisting of a flexible macroglycol akin to poly(tetramethylene oxide) or poly(ε-caprolactone)diol (PCL) within the HPU structure [7].

Again, rapid industrialization through scientific intervention has revolutionized the concept of sustainable development among the global communities. While the basic raw materials, especially petroleum resources are depleting at an alarming rate, genuine efforts are being made to generate naturally renewable alternatives with sustainable attribute [6, 8]. In this milieu, the advancement of bio-based polymers from such renewable resources contributes a noteworthy transformation from conventional petroleum based ones, minimizes risk of adverse effect of non-biodegradability of discarded matter to health and environment, as well as reduces scarcity of raw material and creates ample opportunities of growth and development for the society [9, 10]. Starch, being a versatile and cheap polysaccharide with reactive hydroxyl groups, has found applications as thickener, water soluble binder, emulsifier, gel forming agent and in many non-food items such as paper making, cardboard, textile sizing and adhesives [11, 12]. However, the finished products from native starch suffer from demerits such as, poor processability, low dimensional stability and mechanical properties. It is therefore difficult to achieve the expected level of properties of starch modified polymers to address the demands of many advanced applications. Thus, various physical or chemical

modifications such as blending, derivation and graft copolymerization have been attempted, to develop starch based sustainable polymers with enhanced properties. Also, to attain the desired mechanical properties of such blends some additional agents like glycerol, sorbitol, urea and formamide have to be incorporated [13]. It is therefore difficult to achieve the expected level of properties of starch modified polymers to address the demands of many advanced applications [14, 15]. In this perspective, a simple strategy was reported to use starch as a reactant in a hyperbranched epoxy which was hydrolyzed to obtain hyperbranched polyol. Subsequently, the hyperbranched polyol was used as a branch generating moiety to synthesize HPU with the expectation of high mechanical properties, biocompatibility, biodegradability and almost complete shape recovery near body temperature. The physical and chemical structures of the synthesized HPU were characterized by different spectroscopic and analytical studies. The mechanical (tensile strength, elongation at break, scratch hardness, impact resistance, etc.) and thermal attributes and chemical resistance in different media of the synthesized HPU were evaluated. Moreover, biodegradability, biocompatibility and its endurance as a thermo responsive SMP near body temperature were investigated and discussed in the chapter to emphasize its potential as a safe and smart material for design of biomedical implant devices.

2.2. Experimental

2.2.1. Materials

Polycaprolactone diol (PCL, hydroxyl number 37 mg KOH g^{-1}, density 1.071 g cm^{-3} and number average molecular weight (M_n) 3000 g mol^{-1}) was obtained from Solvay Co., UK. PCL was utilized as a macroglycol in the synthesis of HPU after drying under vacuum for 12 h at 60 °C. Toluene diisocyanate (TDI, molecular weight 174.2 g mol^{-1}, density 1.214 g cm^{-3}, melting point 21.8 °C and boiling point 251 °C) was purchased from Sigma-Aldrich, Germany as a mixture of 20% 2,6- and 80% 2,4- isomers. TDI was employed as received for synthesis of HPU. 1,4-butanediol (BD, density 1.02 g cm^{-3} and minimum assay 99%) was acquired from Merck, Germany. It was employed as a chain extender prior to drying for 12 h under vacuum at 60 °C. Poly(ethylene oxide) glycol with of molecular weight 600 g mol^{-1} (PEG 600, hydroxyl number 178-197, melting point 29 °C and specific gravity 1.13 (at 20 °C)) was procured from Merck, India and

used after vacuum drying at 50 °C for 24 h. Soluble starch (molecular weight 342.30 g mol^{-1}) was acquired from Sigma-Aldrich, Germany. It was employed as a reactant in the synthesis of hyperbranched starch modified polyol (HBSP) after drying under vacuum for 12 h at 60 °C. Bisphenol-A or 4,4'-(propane-2,2-diyl) diphenol (molecular weight 228.29 g mol^{-1}, melting point 159 °C) was obtained from GS Chemicals, India. Bisphenol A was used as a reactant to prepare *in situ* generated diglycedyl ether epoxy of BPA (DGEBA), the monomer (A_2) of hyperbranched starch based epoxy (HBSE). Prior to its use, bisphenol A was purified from toluene by recrystallization. Epichlorohydrin or chloromethyloxirane (molecular weight 92.52 g mol^{-1}, boiling point 117.9 °C and density 1.18 g cc^{-1}) was purchased from GS Chemicals, India. It was used in the preparation of HBSE. Sodium hydroxide (NaOH, molecular weight 40 g mol^{-1} and density 2.13 g cc^{-1}) was used obtained from Merck, India. It was used in the preparation of HBSE, as a base catalyst and in the chemical resistance test for HPU films. NaOH was also employed for the determination of epoxy equivalent values of the synthesized HBSE resins. Potassium hydroxide (KOH, molecular weight 56.11 g mol^{-1}, density 2.12 g cc^{-1} and melting point 406 °C) was purchased from Merck, India and utilized in the determination of hydroxyl value of HBSE and HBSP. Oxalic acid ($C_2H_2O_4$, molecular weight 90.03 g mol^{-1}, density 1.9 g cc^{-1} and melting point 102 °C), an organic dibasic acid, was purchased from Merck, India. It is an organic dibasic acid. It was used for standardization of NaOH and KOH solutions, as the primary standard. Sodium chloride (NaCl, purity 99.5%, molecular weight 58.44 g mol^{-1} and density 2.16 g cm^{-3}) crystals were procured from Merck, India. 10% aqueous solution of NaCl was employed for the chemical resistance test of HPU films. Hydrochloric acid (HCl, molecular weight 36.5 g mol^{-1}) was obtained from Merck, India as 37% (weight by volume) aqueous solution. HCl was used for the determination of epoxy equivalent of the synthesized HBSE and HBSP. A 5% aqueous solution of HCl was used for the chemical resistance test of HPU films. Xylene (molecular weight 106.16 g mol^{-1}, density 0.864 g cm^{-3} and boiling point 138.5 °C) was purchased from Merck, India. Prior to its use as a solvent, xylene was vacuum distilled and kept in 4A type molecular sieves. Molecular sieve (Type: 4A and bulk density: 650-700 g cm^{-3}) was purchased from Merck, India. It consists of alumino-silicate minerals, zeolites, clays, microporous charcoals, porous glasses, synthetic compounds or active carbons with a porous structure through which small molecules can diffuse. Its equilibrium capacity for 75% relative air humidity and water at 30 °C is ≥ 20%. Molecular sieves are employed as received to trap traces of moisture present in solvents.

On the other hand, Alamar Blue (Invitrogen, USA), Dulbecco's Modified Eagle Medium (HDMEM, Gibco, USA), 10% fetal bovine serum (FBS, Gibco, USA), antibiotics (Himedia, India), glutamine (Sigma-Aldrich, USA), phosphate buffered saline (PBS, pH 7.4, Hi-Media, India), calcein AM (Sigma-Aldrich, USA), ethidium homodimer (for dead cells) (Sigma-Aldrich, USA) and TritonX-100 (Sigma Aldrich, USA) were utilized in the biological assessment of HPU films.

Bacterial strain of *Pseudomonas aeruginosa* (*P. aeruginosa*) (Code MTCC 7814), procured from Microbial Type Culture Collection and Gene Bank, Chandigarh, India, was used in the biodegradation study. The bacterial culture was supplied by the Department of Molecular Biology and Biotechnology, Tezpur University, Assam, India.

2.2.2. Methods

2.2.2.1. Preparation of HBSP

Vacuum dried starch, recrystallized bisphenol A and epichlorohydrin (1:3 mol ratio with respect to total hydroxyl groups of starch and bisphenol A) were taken in a two necked round bottomed flask equipped with a condenser, a constant pressure dropping funnel, a magnetic stirrer and a thermometer dipped in an oil bath (**Table 2.1**).

Table 2.1. Composition (mol) of HBSE resins

Reactant	HBSE5	HBSE10	HBSE20
Starch	0.000730	0.00146	0.00292
Bisphenol A	0.0219	0.0219	0.0219
Epichlorohydrin	0.14965	0.1679	0.2044

The reaction was carried out at 100 °C for 5 h under constant magnetic stirring. A 5 N aqueous solution of NaOH (equivalent to the hydroxyl groups) was added drop wise to the reaction mixture through a dropping funnel when the reaction mixture reached to 60 °C. After 5 h from the addition of NaOH, the heating was stopped and allowed to cool down with continued stirring. Once room temperature was attained, the white, viscous product was poured into a separating funnel and was washed with brine solution followed by distilled water for several times to remove the impurities and unreacted reagents that are water soluble. Finally, the HBSE resin was dissolved in THF and vacuum dried at 70 °C to remove excess epichlorohydrin and entrapped water. Using the

same technique, three different compositions of epoxy resins with 5, 10 and 20 wt% of starch were synthesized and coded as HBSE5, HBSE10, HBSE20, respectively. Subsequently, the synthesized HBSE was hydrolyzed with an amount of epoxy equivalent of dilute HCl for about 5 h at 70 °C. The hydrolyzed product (HBSP) was washed with distilled water several times to remove any traces of acid. This was confirmed by adding few drops of $AgNO_3$ solution in the washed off water until there was no formation of white precipitate. The hydrolyzed product was dissolved in THF and dried under vacuum at 70 °C. The hydrolyzed products of HBSE5, HBSE10 and HBSE20 are encoded as HBSP5, HBSP10 and HBSP20, respectively.

2.2.2.2. Synthesis of starch modified polyol-based HPU

HPU was prepared by the pre-polymerization technique in a three-necked round-bottomed flask equipped with a nitrogen inlet, a thermometer, a Teflon septum, and a mechanical stirrer [16, 17]. Required amounts of PCL and DMAc solution of BD were dissolved in the reaction flask in desired amount of xylene under constant stirring. At room temperature, desired amount of TDI was added drop wise into the reaction mixture, maintaining the NCO/OH at 1. The reaction was carried out at 70 ± 2 °C for 3 h in nitrogen atmosphere under constant mechanical agitation to obtain OH terminated pre-polymer. In the second step, HBSP in xylene was introduced to the reaction mixture with the remaining amount of TDI at room temperature (overall NCO/OH = 1). The temperature was maintained at 80 ± 2 °C and stirred continuously for 4 h to complete the reaction as indicated by the absence of the isocyanate band at 2270 cm^{-1} in the FTIR spectrum [3, 16-17]. Using the same technique, three different compositions of PU viz. HPU5, HPU10 and HPU20 were synthesized using HBSP5, HBSP10 and HBSP20 as the branching moiety, respectively. Moreover, linear PU (LPU) was also synthesized following the same technique, except PEG was added in the second step in place of HBSP. Small parts of the synthesized polymers were precipitated in water and dried at 60 °C for 24 h and the rest was cast on a glass slide and a galvanized tin sheet to obtain a film thickness of 1-2 mm for conducting of all other testing and analyses.

2.2.2.3. Sample preparation for performance study

HPU solutions were cast on glass slides (75 mm × 25 mm × 1.39 mm) for gloss and scratch and steel strips (150 mm × 50 mm × 1.44 mm) for impact studies. The coated strips were initially allowed to dry under atmospheric pressure, followed by degassing

under vacuum at 40 °C for 1 h to remove any traces of solvent. The dried films from the glass plates were then peeled off by immersing the plates in warmed distilled water, and subsequently dried under vacuum and stored for 7 days prior to testing.

2.2.2.4. Cell culture and proliferation assay

Primary human dermal fibroblast (HDF) cells were used to study the cell proliferation activity on the polymeric films using the Alamar Blue assay. HDF cells were cultured in high glucose HDMEM supplemented with 10% FBS, Gibco, USA, antibiotics, and 2 mM glutamine. HDF cells were cultured on the variants of PU films such as LPU, HPU5, HPU10 and HPU20. Before culture, the films (10 x 10 x 2) mm were sterilized using 70% v/v ethanol for 4 h and then washed with sterile PBS (pH 7.4) to remove residual alcohol. The polymeric films were preconditioned with HDMEM media for 24 h before seeding the cells. An equal number of cells (2×10^4) were seeded on each film as well as on the tissue culture plate (TCP as the control). Alamar assay was done on the 1st, 3rd, 5th and 7th days following manufacturer's protocol. Briefly, the cell-seeded films were incubated in medium with 10% (v/v) Alamar Blue dye for 3 h at 37 °C in a 5% CO_2 incubator following which 100 mL of solution from each sample was taken and read at 570/600 nm using a multiplate reader (Tecan infinite M 200). Non-seeded films were used as the negative control.

2.2.2.5. Live/dead cell viability assay

Live/dead assay was done to check the viability and adherence of cells on the filmsafter 7 days of culture. The cells were stained using staining solution containing 4 mM calcein AM (for live cells) and 2 mM ethidium homodimer (for dead cells). Briefly, cell-seeded films were rinsed with PBS (pH 7.4) and incubated with live/dead solution for 15-20 min at 37 °C in a humidified incubator. The excess dye was washed with PBS and cells were visualized under a fluorescence microscope. Viable cells convert calcein AM to calcein, which imparts green color to the cells. However, ethidium homodimer enters into dead cells and fluoresces red after binding with DNA.

2.2.2.6. Nucleus staining method

Hoechst staining was done to stain the cell nucleus on the films. The preconditioned sterile films were seeded with HDF cells (2×10^4) and cultured for 7 days in complete HDMEM medium. On the 7th day, the films were washed three times with PBS (pH

7.4), followed by incubation in 3.7% formaldehyde in PBS for 10 min. The samples were further washed with PBS and pre-incubated with 1% BSA for 30 min. The constructs were then made permeable using 0.1% Triton X-100 for 5 min, followed by washing with PBS and staining with 5 mg mL Hoechst 33342 for 30 min. Images were obtained using a fluorescence microscope.

2.2.2.7. Biodegradation study

A biodegradation study was conducted using the McFarland turbidity method using *P. aeruginosa* as the bacterial strain. A medium of mineral salts containing 2.0 g of $(NH_4)_2SO_4$, 2.0 g of Na_2HPO_4, 4.75 g of KH_2PO_4, 1.2 g of $MgSO_4.7H_2O$, 0.5 mg of $CaCl_2.2H_2O$, 100 mg of $MnSO_4.5H_2O$, 70 mg of $ZnSO_4.7H_2O$, 10 mg of $H_3BO_3.5H_2O$, 100 mg of $CuSO_4.7H_2O$, 1 mg of $FeSO4.7H_2O$, and 10 mg of MoO_3, all in 1.0 L of demineralized water, was prepared. It was sterilized for 15 min at 120 °C under a pressure of 15 lb and then allowed to cool to room temperature. The bacterial strain of *P. aeruginosa* was cultured in the medium inside an incubator shaker at 37 °C for 48 h. 100 mL (108 microbes per mL, as calculated using the McFarland turbidity method) of the cultured medium was taken in a conical flask containing 10 mL of the prepared salt medium. The LPU and HPU films were sterilized by autoclaving and were incubated inside the medium under sterile conditions at 37 °C. The flasks containing mineral salt medium but without any bacterial strain were used as the control. The extent of biodegradation was studied from the measurement of weight loss (%) of the degraded LPU and HPU films, measured after 6 weeks of exposure to the bacterial strains, based on the following equation.

$$\text{Weight loss, } W = (W_0 - W_t)/W_t \times 100 \quad \textbf{(Eq. 2.1)}$$

where W_0 and W_t are the weights of the sample before and after degradation, respectively, at the time of interest, t. The bacterial growth is indicated by the increase in turbidity of the medium with time. The optical density (OD) of the microorganism was monitored by measuring the absorbance of the medium at 600 nm with respect to the control. The experiment was performed in triplicate. Scanning electron microscope (SEM) images of the degraded films were taken to study their surface morphology after 6 weeks of bacterial degradation. The test was performed as per ASTM (American Society for Testing and Materials): D 5338-98 standard procedure.

2.2.2.8. Shape memory study

The shape-memory behavior of the LPU and HPU films was studied using the following procedure. Briefly, the films were folded into a spiral shape at 60 °C (~T_m + 20) °C for 5 min, which was immediately immersed into an ice-water salt bath at 15 ± 5 °C for 10 min. The shape fixity of the cooled films was observed by drying them under vacuum and placing at room temperature for 30 min. Consequently, the fixed films were placed in a water bath at 40 °C, for which shape recovery and the time required to retain the original shape was noted. A series of photographs were taken to show the shape-memory effect: (i) original shape, (ii) temporary fixed shape (spiral) at room temperature, (iii)-(v) shapes in a water bath at 40 °C after 5 s, 10 s, and 15 s, respectively, (vi) shape returning to its original form in a water bath at 40 1C after 20 s, and (vii) shape in its original form at room temperature. The shape recovery and shape fixity were calculated from the following equations.

$$\text{Shape recovery (\%)} = [(90 - \theta)/90] \times 100 \quad \textbf{(Eq. 2.2)}$$

$$\text{Shape fixity (\%)} = (\theta/90) \times 100 \quad \textbf{(Eq. 2.3)}$$

where θ in degree denotes the angle between the tangential line at the midpoint of the sample and the line connecting the midpoint and the end of the curved samples. The results are consistent as the test is repeated five times.

2.2.3. Characterization

Fourier Transformed Infrared (FTIR) spectra were recorded on Nicolet (Madison, USA) FT-IR Impact 410 spectrometer in absorbance mode using KBr pellets. ^{1}H Nuclear Magnetic Resonance **(**NMR) and ^{13}C NMR spectra of the polymers were recorded by a 500 MHz AV500 AVANCE-III FT-NMR spectrometer (BROKER, Switzerland), using tetramethylsilane (TMS) as the internal standard and d6-dimethyl sulfoxide **(**d6-DMSO) as the solvents for ^{1}H NMR and ^{13}C NMR, respectively. UV spectra were recorded at room temperature (25 °C) using a Hitachi spectrophotometer (U2001, Tokyo, Japan). Thermal properties were evaluated by thermogravimetric analysis (TGA) and differential scanning calorimetric (DSC) studies. Thermogravimetric study was carried out by using a PerkinElmer 4000 thermal instrument, at 35-700 °C temperature range, at a scanning rate of 10 °C min^{-1}, maintaining an inert atmosphere of nitrogen at a gas flow rate of 30 mL min^{-1}. The DSC study was done by a PerkinElmer DSC 6000, USA instrument in the temperature range -50 to +200 °C (starting temperature = 0 °C) following a cycle of heating-cooling-heating under an atmosphere of nitrogen and at a scanning rate of 3 °C

min^{-1}. Mechanical properties, such as tensile strength and elongation at break were measured by a Universal Testing Machine (UTM, Zwick Z010, Germany) equipped with a 500 N load cell operated at a crosshead speed of 50 mm min^{-1} for tensile strength (ASTM D 638) and elongation at break of samples with dimensions (10 × 1 × 0.02) cm^3. The scratch hardness of the polymeric films was measured by a scratch hardness tester, Model No.705 (Sheen instrument limited, UK) with a stylus accessory at a travel speed of 30-40 mm min^{-1}. The specific gravity of the polymers was assessed with a pycnometer at room temperature (~27 °C) by means of the conventional liquid displacement method (Archemedes' principle). The intrinsic viscosity of the synthesized polymers was determined by Ubbelohde viscometer. The X-ray diffraction (XRD) study was carried out at room temperature (25 °C) by a Rigaku X-ray diffractometer (Miniflex, UK) over a range of 2θ = 10-70 °C. The surface morphology was studied by a scanning electron microscope [SEM, model JSM-6390LV (JEOL)], after platinum coating on the surface. Fluorescently labelled platelets were imaged under a fluorescent microscope (EVOS FL, Life Technologies, USA). Multiplate reader (Tecan, Infinite M200, Switzerland) was used for the determination of the absorbance values in the Alamar Blue assay. The surface morphologies of the biodegraded polymer films and control films (without bacterial strains) were obtained by scanning electron microscopy [SEM, model JSM-6390LV (JEOL)], after platinum coating on the surface.

2.3. Results and discussion

2.3.1. Preparation of HBSP

For obtaining HBSP, synthesis of HBSE resins were conducted first, by poly-condensation reaction using bisphenol A, epichlorohydrin and starch at three different weight percentages of them, keeping the hydroxyl to epichlorohydrin ratio constant, in presence of alkali. At first, diglycidyl ether of bisphenol A was obtained from the reaction mixture, as the reactivity of hydroxyl groups of bisphenol A towards epichlorohydrin is greater than that of starch. The desired hyperbranched epoxy resin was then obtained by the reaction between the diglycidyl ether of bisphenol A and starch. Subsequently, HBSE was hydrolyzed with dilute HCl to form HBSP. The degree of branching (DB) and physical properties for HBSE and HBSP resins are given in **Table 2.2** and **Table 2.3**, respectively.

Table 2.2. Physical properties of HBSE resins

Physical property	HBSE5	HBSE10	HBSE20
Hydroxyl value (g equiv^{-1})	178.46	125.48	149.93
Epoxy equivalent (mg KOH g^{-1})	281.66	206.4	253.35
Yield (%)	96.32	96.6	95.25
Specific gravity	0.9 ± 0.01	1 ± 0.01	1 ± 0.02
Degree of branching	0.63	0.80	0.72

Table 2.3. Physical properties of HBSP resins

Property	HBSP5	HBSP10	HBSP20
Hydroxyl value (mg KOH g^{-1})	328.08	386.56	429.31
Viscosity (dL g^{-1})	0.427	0.376	0.316
Degree of branching	0.63	0.80	0.72

The hydroxyl value of HBSP is higher in comparison to HBSE due to the ring opening reaction of oxirane ring of HBSE on hydrolysis. The hydroxyl value of HBSP20 was the highest due to the presence of the highest wt% of starch (20%) in it. This resulted in a higher percentage of substituted branched epoxide units and subsequently higher number of hydroxyl groups on hydrolysis, as compared to HBSP5 and HBSP10. The DB values of HBSE resins remained unaffected on hydrolysis as only the ring opening reaction of oxirane ring took place. Thus, HBSP resins had the same DB values as their respective HBSE resins on hydrolysis. The viscosity of HBSP20 was the lowest among the other two HBSP resins due to its highest DB that resulted in the formation of highly branched globular type structure bearing no entanglement. HBSP was found to be soluble in most of the organic solvents such as methanol, ethanol, acetone, THF, DMF, DMAc, DMSO, $CHCl_3$, CH_2Cl_2, etc. owing to the presence of a large number of functionalities along with the combination of aliphatic and aromatic moieties in the structures. This further supported the hyperbranched nature of the synthesized polyol. The proposed structure of HBSP20 is shown in **Scheme 2.1**.

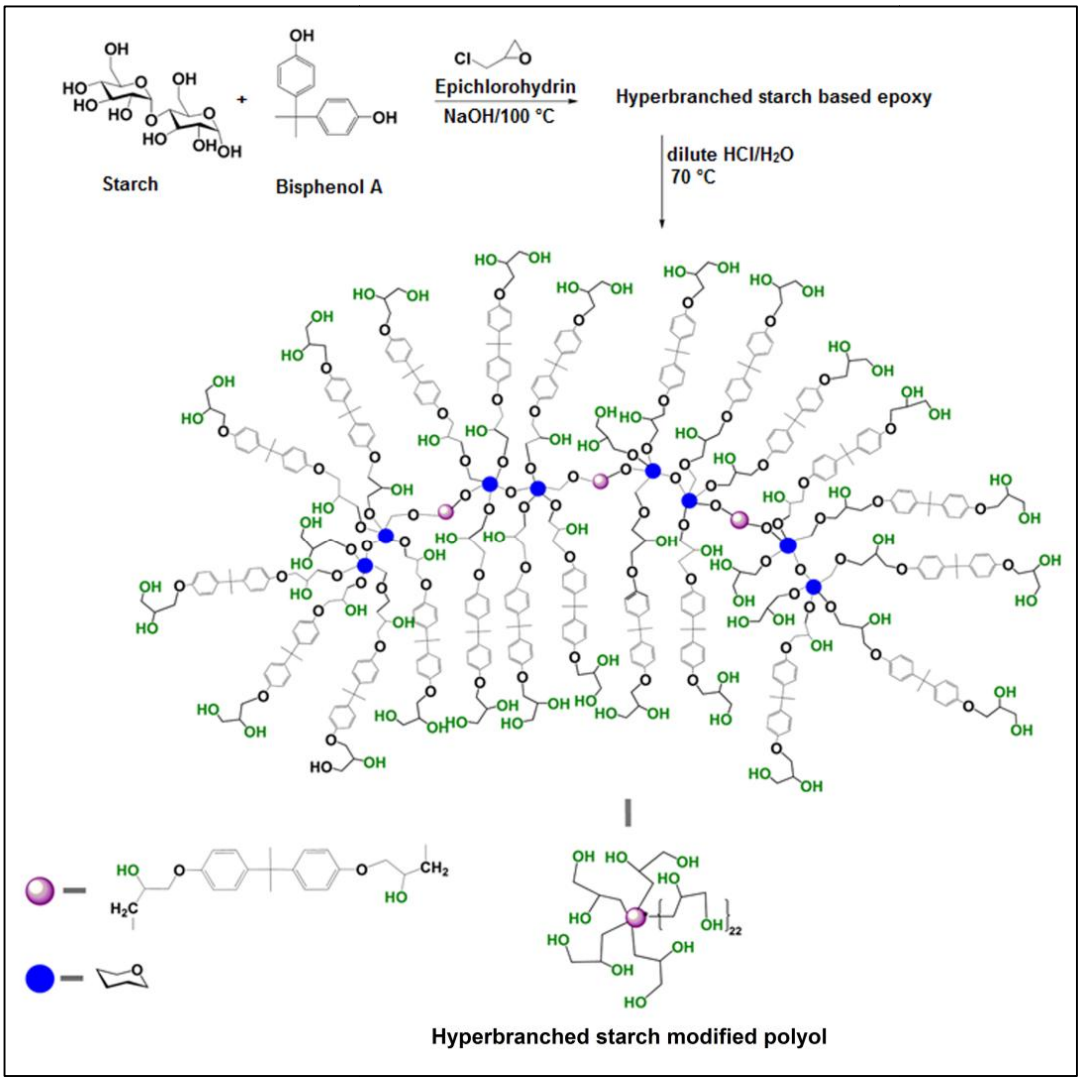

Scheme 2.1. Synthesis of HBSP20.

2.3.2. Characterization of HBSP

2.3.2.1. FTIR analysis

FTIR spectroscopy was used to confirm the variety of chemical functionalities present in HBSP5 (**Figure 2.1)**: ν max/cm^{-1} in FTIR 1604 cm^{-1} (aryl C=C), 3059 cm^{-1} (aryl C-H), 1036 cm^{-1} (alkyl ether), 1247 cm^{-1} (aryl ether) and 3262 cm^{-1} (O-H) [18]. The FTIR spectrum of HBSP shows the disappearance of the sharp band near 912 cm^{-1} (asymmetric vibration of oxirane ring), unlike the spectrum of HBSE. This confirms the ring opening reaction of the oxirane ring on hydrolysis of HBSE by dilute HCl.

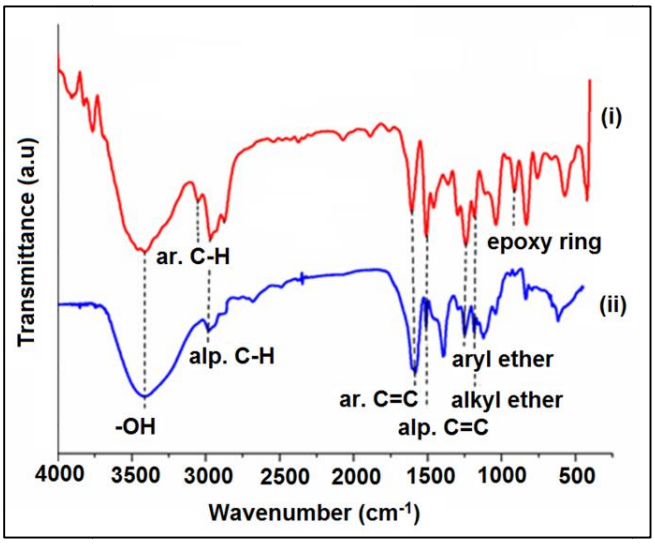

Figure 2.1. FTIR spectra for (i) HBSE5 and (ii) HBSP5.

2.3.2.2. NMR study

The ^{1}H NMR spectrum confirmed the structure of HBSP (**Figure 2.2a**). ^{1}H NMR (δH ppm, 500 MHz, d6-DMSO (S), Me_4Si): 3.8 (1H, CH of secondary hydroxyl group), 3.81 and 3.56 (2H, CH_2 of primary hydroxyl group), 3.9 (2H, CH_2 next to oxirane ring), 6.8 (4H, aromatic protons of bisphenol A), 7.1 (4H, rest aromatic protons of bisphenol A), 1.6 (3H, CH_3 of bisphenol A), 3.7 (2H, CH_2 next to bisphenol A), 4.1 (1H, proton attached with OH), 2.02 (1H, OH), 3.64 (1H, proton attached to C_5 of starch), 3.74 (1H, proton attached to C_6 of starch), 4.95 (1H, proton attached to C_1 of starch), 3.43 (1H, proton attached to C_2 of starch), 2 (1H, OH), 3.39 (1H, proton attached to C_3 of starch),

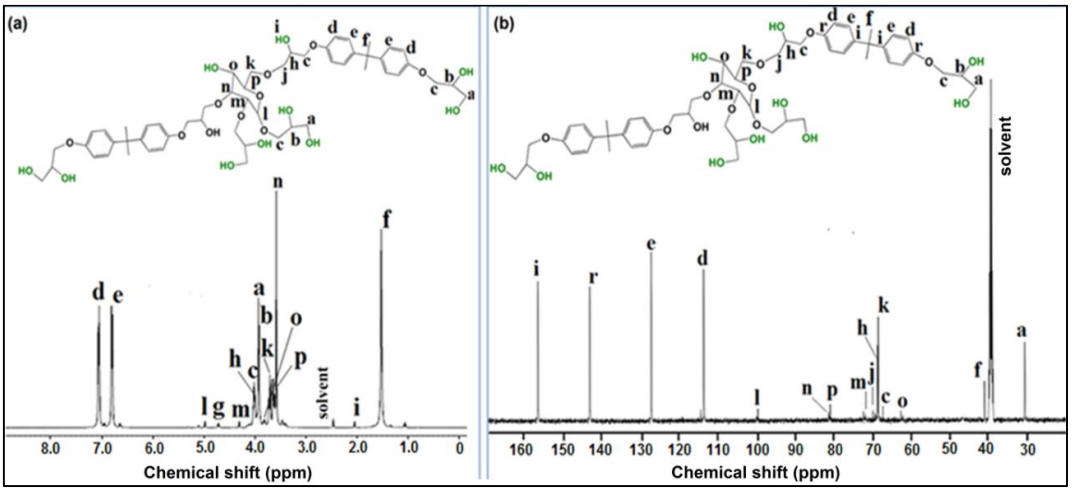

Figure 2.2. (a) ^{1}H NMR spectrum of HBSP20 and **(b)** ^{13}C NMR spectrum of HBSP20.

3.35 (1H, proton attached to C_4 of starch), 5.38 (1H, OH attached to C_4 of starch), 5.58 (1H, OH attached to C_3 of starch). (C_1, C_2, C_3, C_4, C_5 and C_6 of starch are numbered according to the rules of IUPAC and designated as l, m, n, o, p and k, respectively in **Figure 2.2a**).

In the same manner the carbons present in different chemical environments in the structure of HBSP20 were confirmed by ^{13}C NMR spectrum (**Figure 2.2b**). ^{13}C NMR δC, ppm (d6-DMSO, S): 31.04 (CH_3, bisphenol A), 66.7 (carbon of primary hydroxyl group), 71.7 (carbon of secondary hydroxyl group), 69.9 (carbon adjacent to secondary hydroxyl group), 114, 128.9, 143.2, 156.8 (carbons of bisphenol A moiety), 67-100.1 (carbons of starch moiety) [19].

2.3.3. Synthesis of HPU

HPU was synthesized through a two-step, one-pot rearrangement reaction *via* $A_x + B_y$ (x, $y \geq 2$) technique using HBSP as the hyperbranched polyol moiety. The first step involved the formation of -OH terminated pre-polymer (A_2 reactant) through the reaction of macroglycol (PCL) and chain extender (BD) with TDI at the required mol ratio (**Table 2.4**). The multifunctional moiety HBSP as the B_y reactant was added in the second step and the reaction was performed carefully to obtain HPU without gel formation. The addition of HBSP at a relatively elevated temperature, use of the one-shot process and high concentration of HBSP (>15%) led to gel formation.

Table 2.4. Composition (mol) of HPU and LPU

	Eq. functionality of the reactant (mol)			
	HPU5	**HPU10**	**HPU20**	**LPU**
PCL	0.002	0.002	0.002	0.002
HBSP	0.0029	0.0048	0.0068	0
PEG	0	0	0	0.0021
1,4-butanediol	0.004	0.004	0.004	0.004
TDI	0.0089	0.0108	0.0128	0.0081
Hard segment (%)	33	36	39	32
Soft segment (%)	67	64	61	68
HBSP (%)	11	14	17	0

Thus, in the second step, a very dilute solution (15% in xylene) of HBSP was added at room temperature at slow rate. However, when the reaction was run at room temperature or a temperature lower than 80 °C, it did not produce the desired product. Thus, the reaction in the second stage was carried out by a stage wise increase of the temperature up to 80 °C to complete the reaction. The completion of the reaction was confirmed by the absence of -NCO band at 2270 cm^{-1} in FTIR spectrum where the reaction mixture was directly taken from the reactor without any further purification. Further, the butyl amine test confirmed the completion of the reaction [20]. The synthesis of HPU is shown in **Scheme 2.2**.

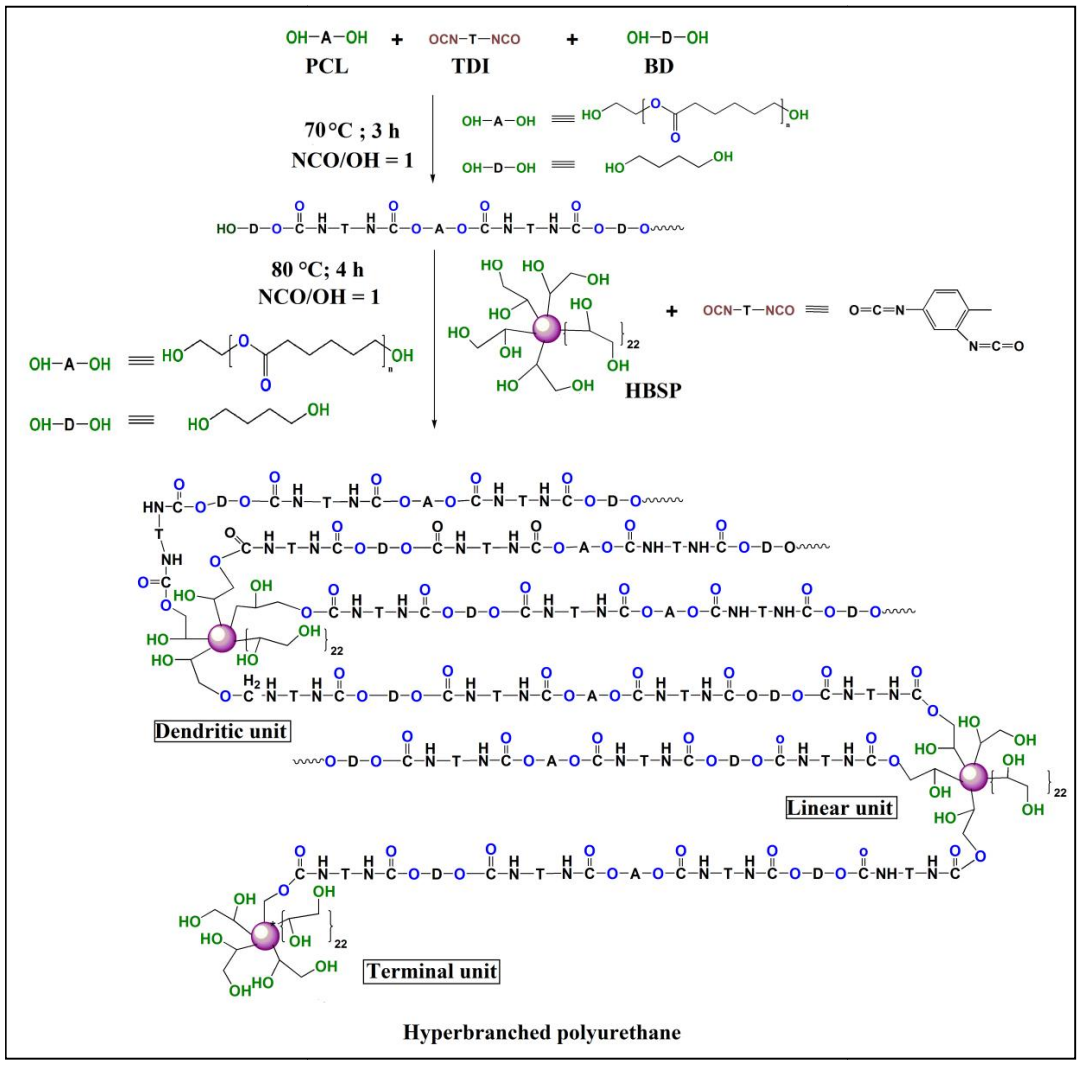

Scheme 2.2. Synthesis of HPU.

2.3.4. Characterization of HPU

2.3.4.1. FTIR analysis

The functional groups of HPU and LPU were confirmed by FTIR analysis (**Figure 2.3)**. The absence of absorption band for free -NCO at 2270 cm^{-1} indicated the completion of the reaction. The absorption band near 3200-3500 cm^{-1} can be attributed to the overlapping of O-H and N-H stretching vibrations. The intensity of O-H and N-H overlapping band for HPU was higher than that of LPU owing to the presence of larger number of surface functionalities and hydrogen bonding (H-bonding).

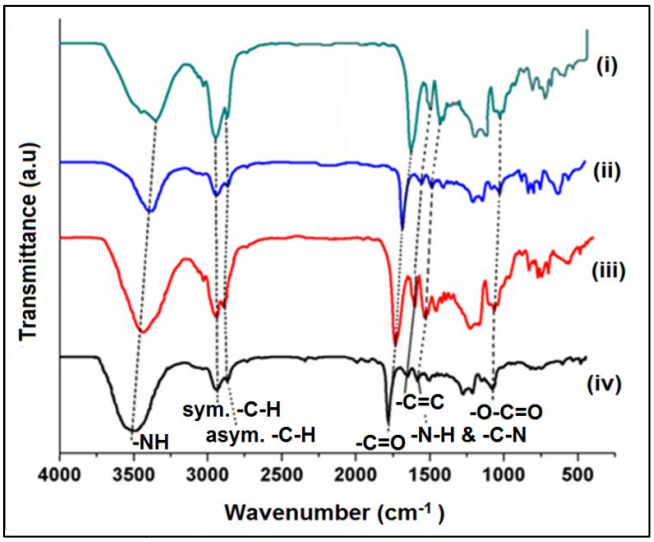

Figure 2.3. FTIR spectra for (i) HPU20, (ii) HPU10, (iii) HPU5 and (iv) LPU.

The bands near 2945-2900 cm^{-1} (asymmetric vibration of CH_2), 2830-2800 cm^{-1} (symmetric vibration of CH_2), 1530-1550 cm^{-1} (C-N stretching/N-H bending vibration), 1040-1060 cm^{-1} (-O-C=O of urethane linkage) and 1710-1730 cm^{-1} (-C=O of urethane linkage) were also found in the spectrum. The N-H/O-H stretching vibration was observed near 3409-3438cm^{-1}. This is mainly due to H-bonding between N-H group and urethane carbonyl, PCL carbonyl or ether oxygen of PCL. A continuous shift of the N-H band from 3438 cm^{-1} to a lower wave number 3409 cm^{-1}, as a function of increase in the amount of TDI was observed in the FTIR spectrum. Similarly, in case of –C=O stretching frequency a gradual shifting from 1710 cm^{-1} to 1685 cm^{-1} was observed with increase in HBSP and starch content. This suggested that with increase in hard segment content the extent of H-bonding increases and demonstrated the different phase separation behavior among PU [3, 21].

2.3.4.2. ^{1}H and ^{13}C NMR study

^{1}H and ^{13}C NMR spectra of HPU20 indicated the presence of urethane linkage, HBSP, butane diol, PCL and TDI moieties. The structure of HPU20 was supported by ^{1}H NMR spectroscopic analysis as shown in **Figure 2.4a.**

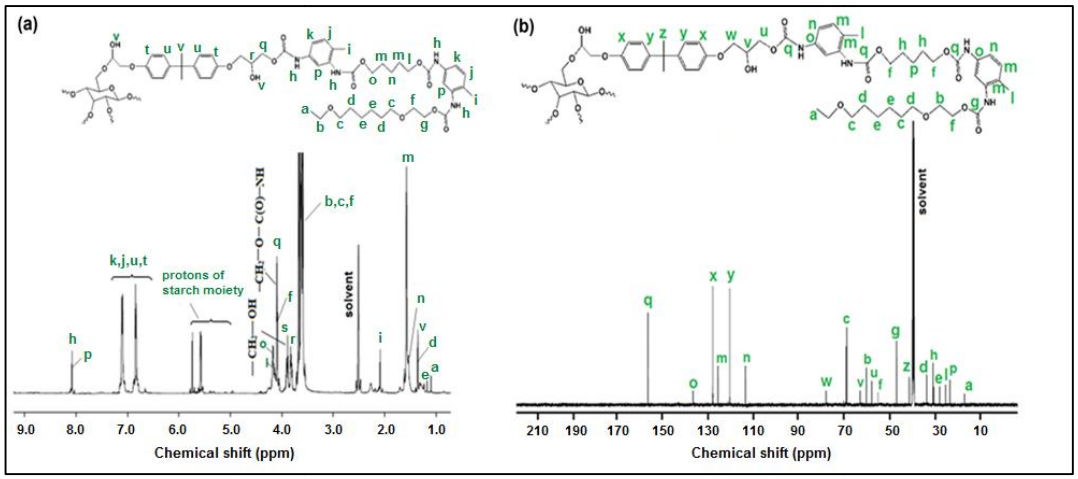

Figure 2.4. (a) ^{1}H NMR spectrum of HPU20 and **(b)** ^{13}C NMR spectrum of HPU20.

In ^{1}H NMR δH, ppm (500 MHz, d6-DMSO (S), Me_4Si): the protons of allylic CH_2, CH_2 adjacent to oxygen atom of urethane group and CH_3 of TDI showed peaks at ∂ = 1.93, ∂ = 2.2 and ∂ = 2.45, respectively. Protons attached to C=C and aromatic protons appeared at ∂ = 5.31 and ∂ = 7-7.6, respectively. Protons attached in aromatic group between two urethane linkages, adjacent to urethane linkage and adjacent to methyl group were found at ∂ = 7.65, ∂ = 7.42 and ∂ = 6.99, respectively [17]. The DB of HPU was calculated by determining the intensity of the peaks of the substituted and un-substituted hydroxyl groups from the ^{1}H NMR spectrum of HPU (**Table 2.2**).

The ^{13}C NMR spectrum also confirmed the structure of HPU20 (**Figure 2.4b**). The chemical shift, δC, ppm (500 MHz, d6-DMSO) of the internal aliphatic carbon peaks of the PCL segment appeared near ∂ = 28. The smaller peak at ∂ = 62.1 is associated with soft-segment carbons that are adjacent to a urethane linkage, while the peak at ∂ = 53.9 is assigned to those soft-segment carbons that are adjacent to oxygen. The peaks near ∂ = 28.4, ∂ = 22.1 and ∂ = 62.7 are attributed to methylene carbons of BD chain extender. The peak around ∂ = 24 is attributed to methyl protons present in TDI. Three different peaks appeared for TDI carbons at ∂ = 135, ∂ = 117 and ∂ = 129 for

aromatic group between two urethane linkages, adjacent to urethane linkage and adjacent to methyl group, respectively [3, 17].

2.3.4.3. SEM image study

The surface morphological studies of HPU and LPU were done by the analysis of SEM images. The SEM image analysis (**Figure 2.5**) revealed that the surfaces of HPU and LPU were not smooth.

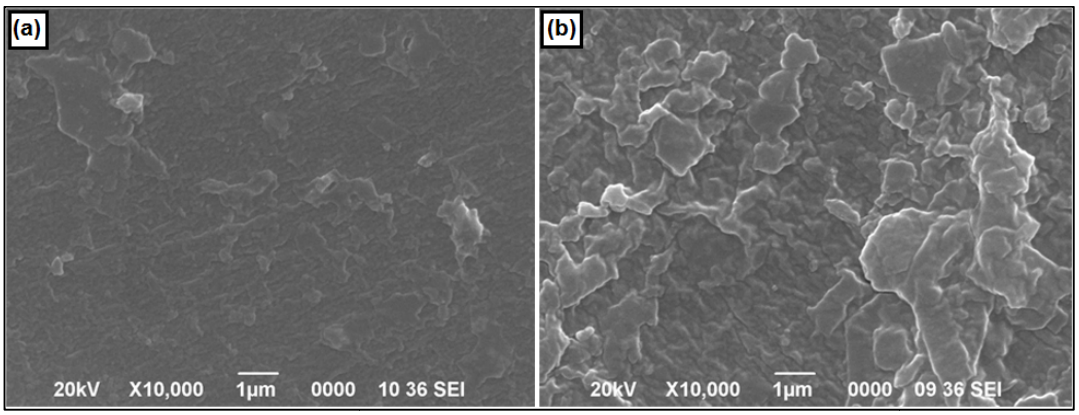

Figure 2.5. SEM micrographs of **(a)** LPU and **(b)** HPU20.

There was a degree of non homogeneity, which may be attributed to the presence of soft and hard segments that leads to phase separation [22, 23]. The observed differences in the surface morphologies of HPU20 and LPU may be due to the difference in the extent of H-bonding in their structures. The presence of multi-functional branching moiety in the hard segment of HPU20 enhanced the H-bonding between hard segment-hard segment as well as hard segment-soft segment and hence the surface of HPU20 was rougher than LPU. The above two factors are responsible for the differences in the surface morphologies of HPU and LPU.

2.3.4.4. XRD pattern study

XRD study of LPU and HPU revealed two strong diffraction peaks near $2\theta = 21.3°$ and $2\theta = 23.4°$ due to the lattice plane corresponding to (100) and (200) of the PCL crystal as shown in **Figure 2.6** [24]. The position of the peaks remained same even after the incorporation of the branching moiety in the PU structure, though the intensity gradually decreased with the increase of HBSP content.

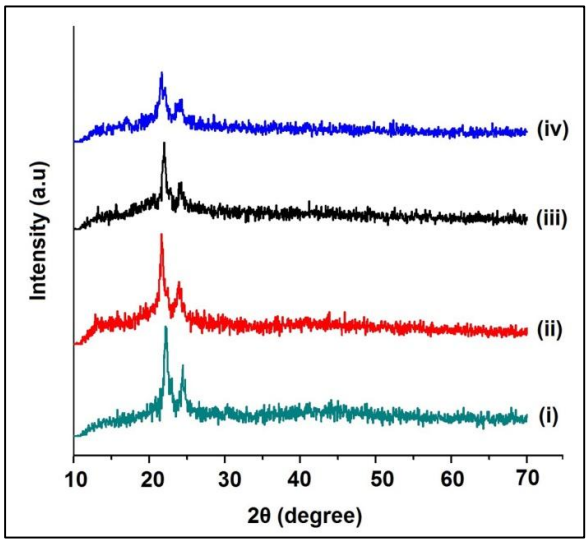

Figure 2.6. XRD patterns of (i) LPU (ii) HPU5 (iii) HPU10 and (iv) HPU20.

This is attributed to the increase in molecular restriction through intermolecular interactions with increase in HBSP content and decrease in the wt% of crystalline PCL moieties in the matrix (**Table 2.2**). This resulted in comparatively less crystallinity in HPU than LPU and the same was supported by DSC study.

2.3.5. Physical properties

One of the most important characteristic of HPU is the solubility. HPU were found to be highly soluble in polar aprotic solvents such as DMF, DMAc, DMSO, THF etc. contrary to LPU, which was partially soluble in some solvents like DMAc, THF etc. This might be attributed to the compact globular structure of HPU and presence of large numbers of polar surface groups [22]. The solution viscosity was slightly higher in LPU than in HPU, owing to the hyperbranched structure of the latter as supported by the DB values (**Table 2.5**). The specific gravity of the PU films varied from 1 to 1.06 with the increase of starch and HBSP content owing to the increase of compactness in the structure, as the number of polar groups increase with the same (**Table 2.5**). However, the values are within the normal range of the PU.

2.3.6. Mechanical properties

Mechanical properties were evaluated for the synthesized HPU and LPU (**Table 2.5**).

Table 2.5. Mechanical and physical properties of HPU and LPU

Property	HPU5	HPU10	HPU20	LPU
Tensile strength (MPa)	13 ± 0.5	15 ± 0.5	17 ± 0.6	9 ± 0.5
Elongation at break (%)	1450 ± 10	1358 ± 8	1158 ± 10	1310 ± 7
Scratch hardness (kg)	5 ± 0.4	5 ± 0.3	6.5 ± 0.2	3.3 ± 0.2
Impact strength (kJ m^{-1})[a]	>19.02	>19.02	>19.02	>19.02
Toughness (MJ m^{-3})[b]	146 ± 5	158 ± 3	163 ± 5	110 ± 6
Specific gravity	1.03	1.05	1.06	1
Degree of branching	0.56	0.65	0.79	-

[a]*Maximum limit of the instrument.*

[b]*Calculated by integrating the area under stress-strain curves.*

Generally, mechanical properties depend on several factors *viz*. presence of H-bonding, polar groups within the polymeric chains, existence of inter and intramolecular interactions, entanglement of chains, compositions and nature of reactants, molecular weight, rigidity of the polymer, etc. [9, 17]. HPU exhibited the highest tensile strength and toughness (calculated from the stress-strain curve) while LPU the lowest as shown in **Figure 2.7**. The tensile strength, scratch hardness and impact resistance increases whereas the elongation at break decreases with increase in wt%. of starch as well as HBSP content in HPU.

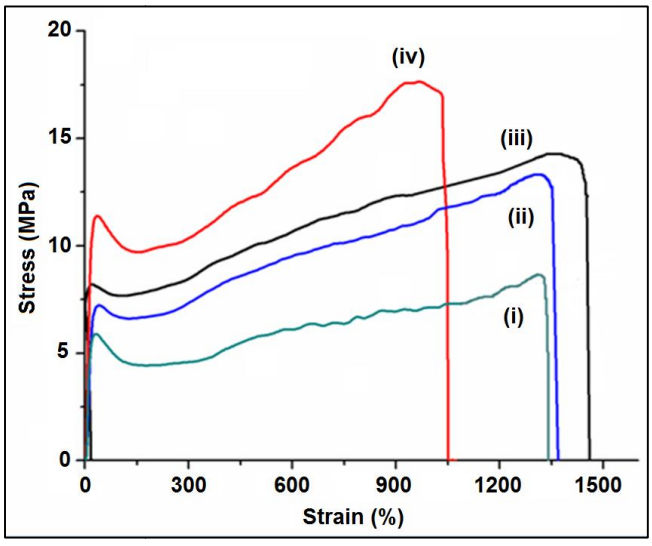

Figure 2.7. (i) Stress-strain profiles of (i) LPU (ii) HPU5, (iii) HPU10 and (iv) HPU20.

The addition of HBSP can favor the above factors by virtue of its rigidity and highly branched structure with polar functional groups as also supported by the DB values (**Table 2.3**). This is due to the predominance of the above factors in HPU in comparison to LPU. HPU20 demonstrated the highest tensile strength and toughness as it contains the highest amount of hard segment as well as HBSP and starch content. This might be due to the increase in inter and intra molecular interactions, degree of H-bonding and amount of aromatic moieties which increased with the hard segment and wt% of starch and HBSP content [3, 9, 17]. Higher elongation at break was displayed by HPU5 and LPU in comparison to HPU10 and HPU20 as the latter exhibits higher DB and possessing compact globular structures. All HPU and LPU films displayed excellent impact strength of 19.02 kJ m^{-1} (maximum limit of the instrument), due to good polymer chain flexibility. The combined effect of aromatic and aliphatic moieties, different intermolecular interactions as well as the highest DB (**Table 2.5**) resulted in the three-dimensional network structure, contributing to the overall excellent performance of HPU20.

2.3.7. Thermal properties

The thermograms and derivatives of the thermograms of HPUs and LPU were studied. In all the cases it was observed that the PU exhibited a two-step thermal degradation pattern (**Figure 2.8)**, as supported by literature [25].

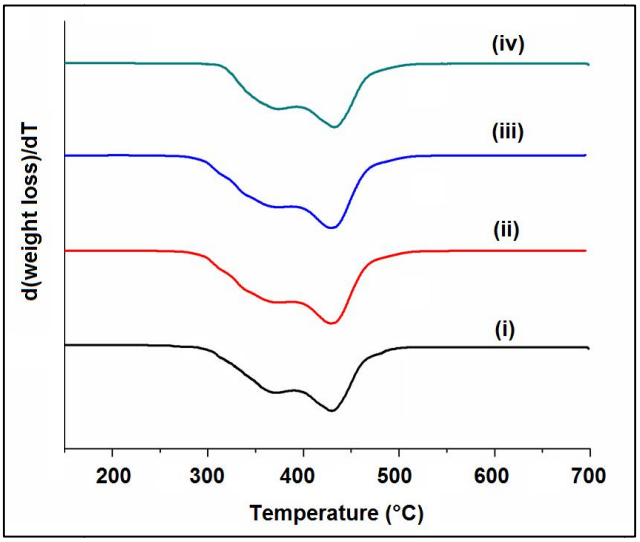

Figure 2.8. DTG curves of (i) LPU, (ii) HPU5, (iii) HPU10 and (iv) HPU20.

The initial degradation temperature, peak temperatures for first and second stages of degradation and char residue at 700 °C are given in **Table 2.6**. The initial degradation temperature ranging from 362-375 °C is attributed to the degradation of thermo labile aliphatic moieties and urethane bonds. HPU exhibited a higher initial degradation temperature than that of LPU as the former possesses a compact hyperbranched structure with a greater number of secondary interactions than the latter. The peak temperature for second step of degradation ranges from 422-438 °C due to the degradation of aromatic rings belonging to TDI and HBSP moieties in HPU and LPU. It is evident from the depicted thermograms, as shown in **Figure 2.9**, that starch and HBSP content in the PU can enhance the thermal stability of HPU, which is consistent with the wt% of starch and HBSP present in the PU (**Table 2.6**).

Table 2.6. Thermal properties of HPU and LPU

Parameter	**HPU5**	**HPU10**	**HPU20**	**LPU**
Onset temperature (°C)	237	262	269	224
1st stage peak degradation (°C)	368	370	375	362
2nd stage peak degradation (°C)	428	432	438	422
Weight residue (%)	2.4	2.9	3.4	1.4
Heat of crystallization (H_c, J g^{-1})	75.18	73.39	70.32	77.36
Crystallinity (%)	55.27	53.89	51.70	56.88
Melting temperature (T_m, °C)	38.03	39.12	40.2	37.9

The hyperbranched structure due to globular confined geometry owing to reactive multi-functional moiety HBSP, enhanced secondary interactions like H-bonding, stronger intra and inter molecular structure contribute towards the thermal properties of HPU in comparison to LPU, where no such moiety was present [19]. It is pertinent to mention here that an overlap of degradation steps was observed which may be due to the fact that during the degradation of aliphatic moieties, especially starch based ones, are transformed to thermostable aromatic moieties through decarboxylation followed by aromatization. This is indirectly supported by the observed higher thermal stability of HPU as compared to LPU imparted by the aromatic moieties as well as enhanced secondary interactions like H-bonding.

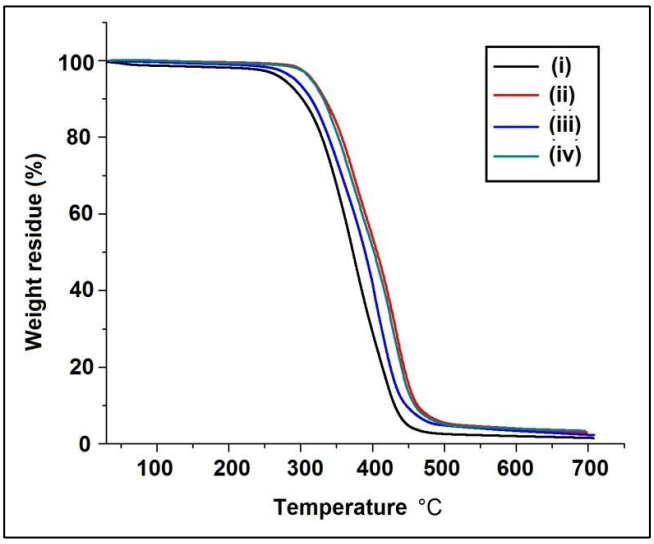

Figure 2.9. TGA thermograms of (i) LPU, (ii) HPU5, (iii) HPU10 and (iv) HPU20.

Further, weight residue left after degradation up to 700 °C also increased with HBSP and starch content due to the formation of carbonaceous products. The melting transition temperature (T_m) and heat of crystallization (H_c) of HPU and LPU were measured with the help of DSC as given in **Table 2.6** and shown in **Figure 2.10**.

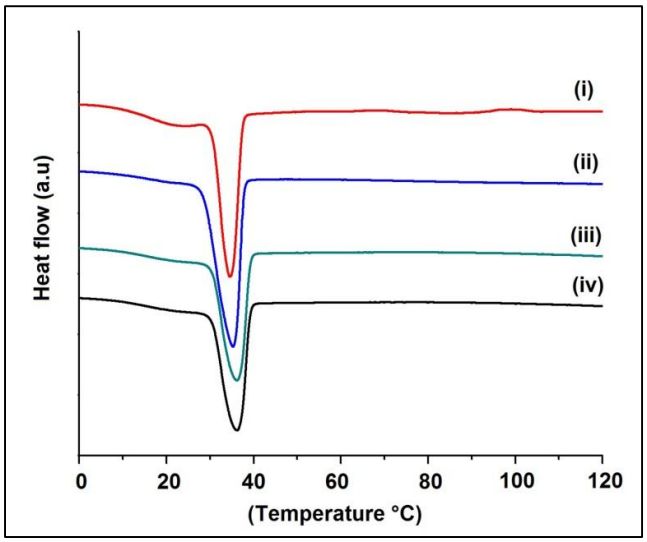

Figure 2.10. DSC curves of (i) HPU20, (ii) HPU10, (iii) HPU5 and (iv) LPU.

The crystallinity of the soft segments of HPUs were determined by the measurement of H_c on cooling and with an enthalpy value of 136 J g^{-1} for 100% crystalline PCL. The T_m of HPU increased with an increase in HBSP and starch content which leads to the

formation of a compact structure through various types of interactions. This is due to the fact that starch exhibits a hydrophilic property which in turn leads to a large number of intramolecular interactions and strong intermolecular associations *via* H-bonding formed by the hydroxyl groups in the structure [11].

2.3.8. Cell proliferation assay

Greater Alamar blue reduction directly relates to enhanced cellular metabolism and cell proliferation on the films [26]. The results show enhanced cell proliferation in HPU films containing starch as well as HBSP, as compared to LPU with no starch or HBSP content. In comparison to 1st day, cell proliferation on HPU20 films showed a 3-fold increment on 7th day. On other film variants the yield varied between~2.5-fold for HPU10 and~2.3 fold for HPU5 and LPU with $p \leq 0.01$ (**Figure 2.11**).

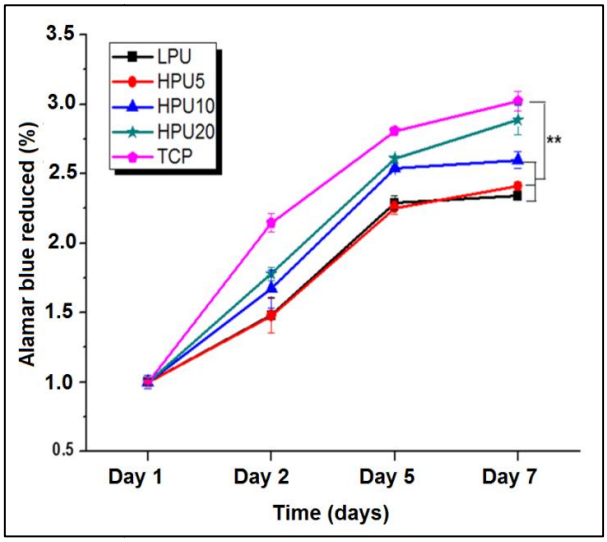

Figure 2.11. Alamar Blue cell proliferation assay showing HDF cell proliferation on HPU and LPU films. Data are plotted as means ± standard deviation. (**$p < 0.01$, n = 3).

The cellular growth was observed to increase with the HBSP and starch content in PU. On day 7, HPU20 (containing 20 wt% of starch and 17 wt% HBSP content) films showed the maximum cell growth with higher Alamar reduction reaching close to TCP control values followed by HPU10 (10 wt% of starch and 14 wt% of HBSP); HPU5 (5 wt.% of starch and 11 wt% of HBSP) and LPU (without starch or HBSP content). There was significant difference between the TCP compared with LPU, HPU5 and HPU10 ($p <$ 0.01). However, no significant difference was observed between TCP and HPU20 ($p >$

0.01). This effect may be due to the presence of higher amount of starch based polyol and starch content in HPU20. Starch supports cellular growth and is widely reported as biodegradable material for a range of biomedical applications including tissue engineering scaffold [27], bone cements or drug delivery carriers [28]. The assay results indicate that the different films are cytocompatible for varied biological applications.

2.3.9. Live/dead cell viability assay

Live/dead assay was performed to evaluate cellular viability and adhesion. As evident from fluorescent microscopic images, HDF cells were found to uniformly distribute and firmly adhere on the films (**Figure 2.12**).

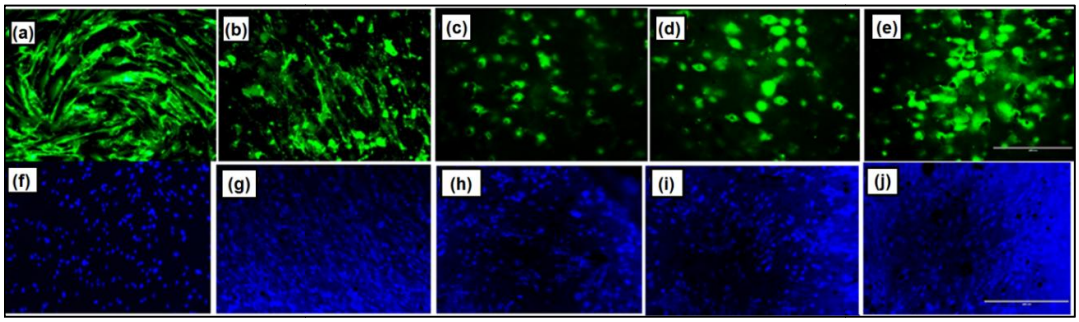

Figure 2.12. Fluorescent microscopic images of live/dead **(a-e)** and Hoechst **(f-j)** staining showing human dermal fibroblast (HDF) cells growing on films after seven days of culture. **(a, f)** tissue culture plate (TCP), **(b, g)** LPU **(c, h)** HPU5 **(d, i)** HPU10 and **(e, j)** HPU 20. *Scale bar represents 400 mm.

In comparison to control and LPU films where cells were found in their native spindle shape, HPU films exhibited rounded cell clusters (**Figure 2.12c-e**) which may be an effect of starch and starch based polyol, present in the structure. However, in all films no dead cell was observed after 7 days of culture suggesting material biocompatibility. Similarly, on staining with Hoechst dye prominent, rounded healthy nucleus were observed on all films distributed throughout (**Figure 2.12f-j**). This reaffirms that the material is highly biocompatible and can be used for various biomedical applications.

2.3.10. Biodegradation study

From the biodegradation study of HPU and LPU films, it was established that they were regularly degraded on exposure time by *P. aeruginosa* bacterial strain (**Figure 2.13**). The

differences in the cell wall structure of the gram negative bacteria, *P. aeruginosa* acts as an active barrier which is supposed to control the degradation of the polymer substrate. It was found that the PU films were degraded to a considerable amount after 6 weeks of inoculations by the used bacterial strain. This signifies that the polymer (carbon source) acted as catabolite to the bacteria [29]. The degradation was rapid for HPU in comparison to that of LPU. Thus, HPU were more susceptible to bacterial degradation. The well exposed and expanded hyperbranched structure of HPU compared to LPU is more favorable for the attachment of the bacterial strain to form a bio-film which easily metabolized HPU for extraction of nutrients.

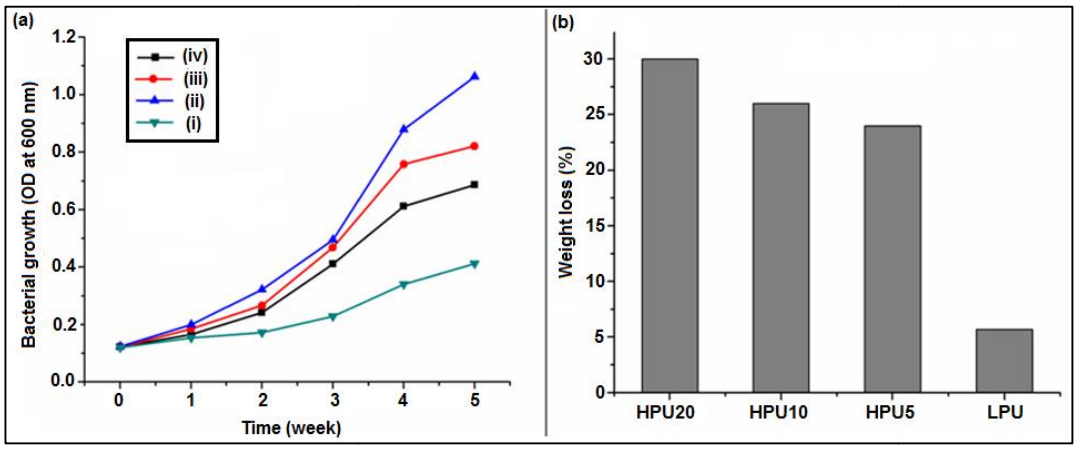

Figure 2.13 (a) Variations of *P. aeruginosa* bacterial growth against exposure time for PU and **(b)** Weight losses of PU films after 60 days of exposure to the *P. aeruginosa* bacterial strain.

The growth of the bacterial strain was found to be the highest for HPU20, as it contains the highest amount of starch in its structure, and thus provides a better susceptible surface for bacterial growth, as evident from the OD curves (**Figure 2.13a**). The weight losses of the PU films were found after 6 weeks of exposure to the bacterial strain which showed reduction in their weights. This is due to biodegradation of starch by microorganism attack [30]. Also, as HPU20 consisting of the highest amount of starch in its structure, it exhibited the highest weight loss of 30% after 6 weeks of their exposure to the bacterial strain as shown in **Figure 2.13b**. The SEM images also revealed that HPU20 had undergone significant surface erosion and bacterial adherence as compared to LPU in the same time period by *P. aeruginosa* (**Figure 2.14**). This may be due to the globular, confined structural geometry of HPU20 which is favorable for the easy

penetration of the bacterial strain within the macromolecular structure of the PU as their food source. The surface of the LPU film displayed only slight surface erosion (**Figure 2.14**) as compared to HPU20 due to the absence of starch content and presence of only biodegradable PCL moiety in the structure of LPU. Therefore, HPU exhibited enhanced biodegradation compared to LPU. Thus, all HPU are biodegradable and the rate of biodegradation of all three HPU depended on the starch and HBSP content.

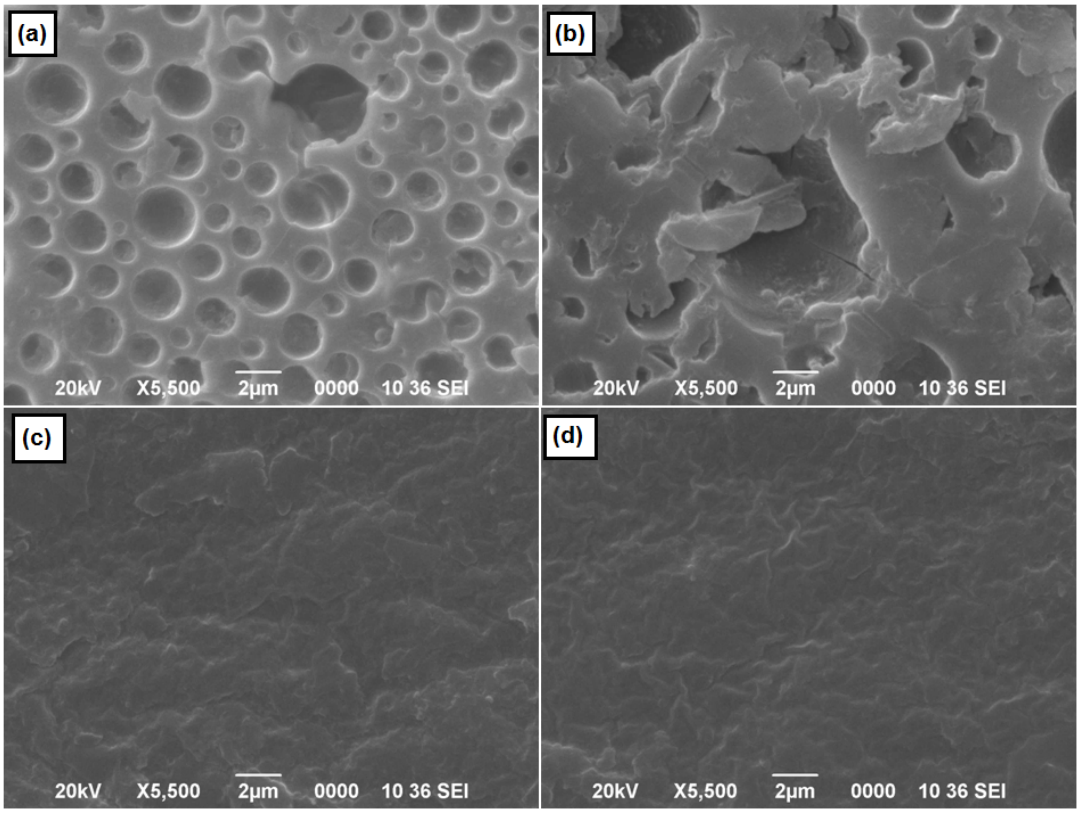

Figure 2.14. SEM images of **(a)** HPU20 and **(b)** LPU after biodegradation; and **(c)** HPU20 and **(d)** LPU before biodegradation.

2.3.11. Shape-memory study

The shape memory behaviors of the PU films near body temperature are shown in **Figure 2.15**. The shape memory effect of SMP is predominantly an entropic process. In the permanent shapes of the HPU and LPU films, the polymer chains are oriented in a random coil formation *i.e.*, at their highest entropic state.

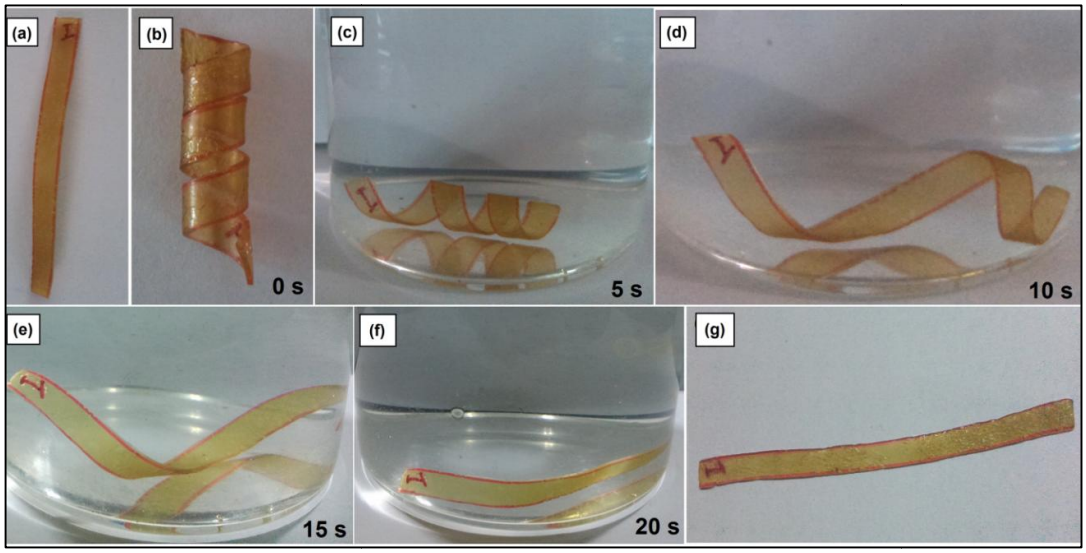

Figure 2.15. Shape-memory effect of HPU20 film. **(a)** Original shape, **(b)** Fixed shape at room temperature **(c)** to **(e)** shapes in water bath at 40 °C after 5 s, 10 s, 15 s, respectively **(f)** Shape returning to original form in water bath at 40 °C after 20 s, and **(g)** Shape in its original form at room temperature.

When the PU samples are heated above their shape memory transition temperature at 60 °C (T_m + 20), chain mobility is activated. Thus, they can be easily deformed into a temporary spiral shape, and their entropic state is lowered. The spirally folded HPU and LPU samples were then quenched into an ice salt bath, to fix the temporary spiral shape by kinetically freezing the polymer's molecular chains. Subsequently, when the mechanical stress was removed the polymer chains did not have sufficient energy to reverse the deformation. Upon reheating the PU samples above their T_m, the molecular chain mobility is reactivated which allows the chains to gain entropy and return to the random coil motion [31]. The shape recovery of the HPU films was increased with the increase in wt% of HBSP (**Table 2.7**). The better shape recovery of HPU compared to LPU is attributed to the increased stored energy of system.

Table 2.7. Shape memory properties of HPU and LPU

Property	HPU5	HPU10	HPU20	LPU
Shape recovery (%)	96.5 ± 0.1	97.7 ± 0.2	98.9 ± 0.1	93.3 ± 0.1
Shape fixity (%)	96.2 ± 0.2	97.6 ± 0.3	98.8 ± 0.1	70 ± 0.2
Shape recovery time (s)	21 ± 1	21 ± 1	20 ± 1	25 ± 1

This is due to uniform distribution of hard segments, multifunctional moiety HBSP and increased secondary interactions in the structure of HPU [32, 33]. HPU also exhibited better shape fixity compared to LPU due to the hyperbranched structure of the former that enhanced the secondary interactions and the physical or virtual cross-links among the new orientated polymer segments upon cooling.

Thus, by deforming such heat sensitive SMPs above their T_m, a desired fit can be obtained and sustained after cooling. Therefore, such SMP can possess potential biomedical applications in designing minimally invasive smart implants.

2.4. Conclusion

The present study reported the synthesis of biodegradable HPU using a starch modified hyperbranched polyol as a bio-based material with excellent yield, through a facile approach. The polymer exhibited remarkable mechanical performance, high thermal stability, good biodegradability and exceptional shape recovery near body temperature. Furthermore, cell proliferation and live/dead cell viability assays confirmed the biocompatibility of the polymer. Thus, the starch modified polyol based tough biodegradable, biocompatible hyperbranched polyurethane has potential applications as an excellent physiological temperature responsive SMP in advanced biomedical field.

References

[1] Deka, H., Karak, N., Kalita, R. D., and Buragohain, A. K. Biocompatible hyperbranched polyurethane/multi-walled carbon nanotube composites as shape memory materials. *Carbon*, 48(7):2013-2022, 2010.

[2] Lendlein, A., Jiang, H. Y., Junger, O., and Langer, R. Light-induced shape-memory polymers. *Nature*, 434:879-882, 2005.

[3] Thakur, S. and Karak, N. A tough, smart elastomeric bio-based hyperbranched polyurethane nanocomposite. *New Journal of Chemistry*, 39(3):2146-2154, 2015.

[4] Lendlein, A. and Langer, R. Biodegradable, elastic shape-memory polymers for potential biomedical applications. *Science*, 296(5573):1673-1676, 2002.

[5] Li, X., Fang, Z., Li, X., Tang, S., Zhang, K., and Guo, K. Synthesis and application of a novel bio-based polyol for preparation of polyurethane foams. *New Journal of Chemistry*, 38(8):3874-3878, 2014.

[6] Thakur, S. and Karak, N. Castor oil-based hyperbranched polyurethanes as advanced surface coating materials. *Progress in Organic Coatings*, 76(1):157-164, 2013.

[7] Unal, S., Yilgor, I., Yilgor, E., Sheth, J. P., Wilkes, G. L., and Long, T. E. A new generation of highly branched polymers: hyperbranched, segmented poly(urethane urea) elastomers. *Macromolecules*, 37(19):7081-7084, 2004.

[8] Tschan, M. J. L., Brule, E., Haquette, P., and Thomas, C. M. Synthesis of biodegradable polymers from renewable resources. *Polymer Chemistry*, 3(4):836-851, 2012.

[9] Gogoi, S. and Karak, N. Biobased biodegradable waterborne hyperbranched polyurethane as an ecofriendly sustainable material. *ACS Sustainable Chemistry & Engineering,* 2(12):2730-2738, 2014.

[10] Russell, D. A. M. and Shiang, D. L. Thinking about more sustainable products: using an efficient tool for sustainability education, innovation, and project management to encourage sustainability thinking in a multinational corporation. *ACS Sustainable Chemistry & Engineering,* 1(1):2-7, 2013.

[11] Lu, D. R., Xiao, C. M., and Xu, S. J. Starch-based completely biodegradable polymer materials. *Express Polymer Letters*, 3(6):366-375, 2009.

[12] Dave, H., Rao, P. V. C., and Desai, J. D. Biodegradation of starch-polyethylene films in soil and by microbial cultures. *World Journal of Microbiology and Biotechnology,* 13(6):655-658, 1997.

[13] Lu, Y. and Tighzert, L. Novel plastics and foams from starch and polyurethanes. In *Biodegradable Polymer Blends and Composites from Renewable Resources*, pages 87-105, ISBN:9780470391501. John Wiley & Sons, Inc., 2008.

[14] Da Roz, A. L., Curvelo, A. A. S., and Gandini, A. Preparation and characterization of cross-linked starch polyurethanes. *Carbohydrate Polymers*, 77(3):526-529, 2009.

[15] Kim, M. and Lee, S. J. Characteristics of crosslinked potato starch and starch-filled linear low-density polyethylene films. *Carbohydrate Polymers*, 50(4):331-337, 2002.

[16] Kalita, H. and Karak, N. Biobased hyperbranched shape-memory polyurethanes: effect of different vegetable oils. *Journal of Applied Polymer Science*, 131(1):39579-39586, 2014.

[17] Das, B., Konwar, U., Mandal, M., and Karak, N. Sunflower oil based biodegradable hyperbranched polyurethane as a thin film material. *Industrial Crops and Products*, 44:396-404, 2013.

[18] De, B., Gupta, K., Mandal, M., and Karak, N. Biodegradable hyperbranched epoxy from castor oil-based hyperbranched polyester polyol. *ACS Sustainable Chemistry & Engineering*, 2(3):445-453, 2013.

[19] Jordan, T., Schmidt, S., Liebert, T., and Heinze, T. Molten imidazole - a starch solvent. *Green Chemistry*, 16(4):1967-1973, 2014.

[20] Karak, N., Rana, S., and Cho J. W. Synthesis and characterization of castor-oil-modified hyperbranched polyurethanes. *Journal of Applied Polymer Science,* 112(2):736-743, 2009.

[21] Deka, H. and Karak, N. Bio-based hyperbranched polyurethanes for surface coating application. *Progress in Organic Coatings,* 66(3):192-198, 2009.

[22] Karak, N. *Fundamentals of Polymers: Raw Materials to Applications*. PHI Learning Pvt. Ltd., New Delhi, 2009.

[23] Prisacariu, C. *Polyurethane Elastomers: From Morphology to Mechanical Aspects*. Springer, Vienna, 2011.

[24] Sahoo, N. G., Jung, Y. C., Yoo, H. J., and Cho, J. W. Effect of functionalized carbon nanotubes on molecular interaction and properties of polyurethane composites. *Macromolecular Chemistry and Physics*, 207(19):1773-1780, 2006.

[25] Javni, I., Petrovic, Z. S., Guo, A., and Fuller, R. Thermal stability of polyurethanes based on vegetable oils. *Journal of Applied Polymer Science*, 77(8):1723-1734, 2000.

[26] Mandal, B. B., Grinberg, A., Gil, S. E., Panilaitis, B., and Kaplan, L. D. High-strength silk protein scaffolds for bone repair. *Proceedings of the National Academy of Sciences of the United States of America,* 109(20):7699-7704, 2012.

[27] Salgado, A. J., Coutinho, P. O., and Reis, L. R. Novel starch-based scaffolds for bone tissue engineering: cytotoxicity, cell culture, and protein expression. *Tissue engineering*, 10(3-4):465-474, 2004.

[28] Pereira, C. S., Cunha, M, A., Reis, L. R., Vazquez, B., and Roman, S. J. New starch-based thermoplastic hydrogels for use as bone cements or drug-delivery carriers. *Journal of Materials Science: Materials in Medicine,* 9(12):825-833, 1998.

[29] Priya, T. and Usharani, G. Comparative study for biosurfactant production by using *Bacillus subtilis* and *Pseudomonas aeruginosa*. *Botany Research International*, 2(4):284-287, 2009.

[30] El-Sheshtawy, H. S. and Doheim, M. M. Selection of *Pseudomonas aeruginosa* for biosurfactant production and studies of its antimicrobial activity. *Egyptian Journal of Petroleum*, 23(1):1-6, 2014.

[31] Lin, T., Tang, Z., and Guo, B. New design strategy for reversible plasticity shape Memory polymers with deformable glassy aggregates. *ACS Applied Materials & Interfaces*, 6(23):21060-21068, 2014.

[32] Meng, Q., Hu, J., Ho, K., Ji, F., and Chen, S. The shape memory properties of biodegradable chitosan/poly(L-lactide) composites. *Journal of Polymers and the Environment*, 17:212-224, 2009.

[33] Chun, B. C., Cho, T. K., and Chung, Y. C. Blocking of soft segments with different chain lengths and its impact on the shape memory property of polyurethane copolymer. *Journal of Applied Polymer Science*, 103(3):1435-1441, 2007.